Prediction of part distortion in Fused Deposition Modelling (FDM) of semi-crystalline polymers via COMSOL: Effect of printing conditions

Anto Antony Samy[a]*, Atefeh Golbang[a], Eileen Harkin-Jones[a], Edward Archer[a], Alistair McIlhagger[a]

a: Engineering Research Institute, Ulster University, Shore Road, Newtownabbey, Co. Antrim, BT37 0QB, United Kingdom

Abstract

Residual stresses and warpage adversely affect the dimensional accuracy and performance of 3D-printed semi-crystalline polymers in Fused Deposition Modelling (FDM). One of the main challenges in FDM is to understand and relate the impact of printing conditions on part distortion for optimizing the 3D-printing process to achieve good print quality. Hence, the effect of various printing parameters, particularly print bed temperature, layer bonding, layer thickness and raster pattern, on built-up residual stresses and warpage is simulated in this work, by building a relationship between the crystallisation kinetics, viscoelastic and thermo-mechanical properties of the polymer in relation to changes in temperature during FDM using element activation in COMSOL. To the best of our knowledge, this is a novel approach for quantitative prediction of part distortion in FDM of semi-crystalline polymers under various printing conditions. Based on the simulation results, it is observed that a decrease in layer thickness from 0.5mm to 0.1mm results in an 89% drop in warpage and a reduction in residual stress of 24%. Applying a line raster pattern reduces warpage and residual stresses by 16% and 36%, respectively in comparison with a zigzag raster pattern. Very good agreement is observed between simulation and experimental results for warpage under various printing conditions. The results of this study can be used to predict and/or minimise part distortion in a semi-crystalline, 3D-printed polymer by simulating the effect of printing parameters on residual stresses during FDM.

Keywords

Finite Element Analysis (FEA), Fused Deposition Modelling (FDM), semi-crystalline polymers, warpage, simulation, 3D printing.

1. Introduction

Additive manufacturing (AM) or 3D printing is an advanced manufacturing process that builds parts layer by layer using a wide range of material such as plastics, ceramics and metals [1]. Among the various AM methods, Fused Deposition Modelling (FDM) has shown great potential because of its ability to print parts with complicated geometry [2], simplicity of

operation and cost efficiency. FDM is basically an extrusion system that operates with a travelling nozzle, depositing molten material, layer-by-layer, on the print bed. It has the ability to produce parts with complicated structures and intricate details. However, the build-up of residual stresses during the printing process can result in dimensional inaccuracy and reduction in mechanical properties. Since the thermal residual stresses are dependent on temperature fluctuations, changes in the printing conditions can significantly impact the quality and dimensions of the printed parts. In other words, the structural integrity of the part is compromised if high amounts of residual stresses are induced during 3D-printing. The final mechanical properties are also affected by warpage; the threshold for cracking/breaking of the part is reduced under external load [3,4].

FDM is becoming more attractive for various applications in aerospace, automotive, and biomedical applications. With increase in the application of plastics and polymer composite material in various fields, polymers have become one of the most commonly used materials for 3D printing [5]. Among the thermoplastic feedstocks for FDM, semi-crystalline polymers are increasingly gaining attention. This is due to their excellent mechanical properties in high temperature environments, and their chemical and wear resistance properties [6,7]. However, semi-crystalline polymers are more prone to thermal shrinkage and warpage compared with amorphous polymers. This is due to the microstructural changes occurring in a semi-crystalline polymer during phase transition (crystallisation) through ordering of long polymer chains. Hence, 3D printing of semi-crystalline polymers via the FDM process is often more complicated and highly dependent on printing conditions [2,8].

In FDM of semi-crystalline polymers, the residual stresses occur for a number of reasons. During the cooling phase, the deposited polymer melt cools down from the extrusion temperature to ambient temperature. The outer surface cools at a much faster rate than the core. This imbalance in the thermal profile, gives rise to a compressive stress on the outer surface while a tensile stress is formed inside the polymer to counter balance, resulting in anisotropic contraction (shrinkage), build-up of internal residual stresses and warpage [9–12]. Additionally, due to the poor conductive nature of polymers, the non-homogeneous thermal distribution through the deposited layers leads to non-uniform cooling, further increasing the residual stress and distortion (shrinkage/warpage) of the printed part [13]. One of the important sources of residual stress in processing of semi-crystalline polymers is crystallisation. The degree of crystallinity in the polymer is influenced by the cooling rate, with slower cooling leading to greater crystallinity and changes in density, hence higher residual stresses and warpage. [14,15].

In recent times, an increasing number of researchers have been focusing on reducing or controlling the amount of shrinkage and warpage in FDM of semi-crystalline polymers through tailoring of processing conditions and material properties via process simulations and experimentation [2,8,16–23]. It has been shown that residual stresses and warpage in a semi-crystalline polymer are highly influenced by the degree of crystallisation [24], thermo-mechanical properties, viscoelastic nature, relaxation behaviour [25], and volumetric shrinkage of the material. Printing parameters such as print bed temperature, layer thickness [26], ambient temperature [22], etc., also have a significant impact on the final print quality and part distortion. Zhang et al. [2,8] studied the thermal behaviour of a 3D printed part via FDM by focusing on the impact of tool path, nozzle speed, and layer thickness on the built-in residual stresses. They concluded that layer thickness and nozzle speed have a direct effect on the part distortion. Later, Zhang et al. [16] performed a cooling study of the printed part and arrived at similar conclusions.

Modelling and simulation of the FDM process can be used as an effective tool for providing insight into the relationship between shrinkage/warpage and printing conditions in order to achieve good print quality without significant trial and errors experimentation, hence, saving time, money and energy. Hence, researchers are attempting to simulate shrinkage and warpage in 3D printed parts. In most cases, the data from previous experimental studies are used for modelling and simulation. However, the impact of various printing conditions on the residual stresses and part distortion is not yet fully addressed and often lack accuracy [2,8,16,27,28].

Courter et al. [29] studied the effects of residual stresses in their simulation. Material properties such as specific heat capacity was considered temperature dependent, and the part was assigned with a fixed temperature boundary condition for a print bed for simplification purposes. Ramanath et al. [30], Anthony et al. [31] and Shahriar et al. [32] investigated the effects of coupled thermal diffusion with fluid dynamics in a polymer material. Ramanath et al. investigated the melt flow behaviour of polymers in FDM and reported that a nozzle diameter of 0.3mm produced desirable material flow characteristics and was in good agreement with the numerical results. The results obtained for rapid cooling simulation in the study by Anthony et al. were higher than the experimental data. This was because a uniform thermal distribution was assumed from the nozzle to the layers and the build plate. In the study carried out by Shahriar et al. thermal and fluid flow physics were coupled to investigate the crystallisation kinetics of PEEK and PLA. The researchers suggested that the nozzle gap and ambient temperature control could be the key to minimising deformation in the polymers [32].

From the literature, it is apparent that the major source of discrepancy in the FDM simulations for prediction of warpage in semi-crystalline polymers, is due to neglect of the crystallisation kinetics and assuming that the material properties of the polymer are invariable with processing conditions [33]. The recently developed model by Brenken et al. shows a significant improvement in terms of predicting built-in residual stresses and part distortion by including the crystallisation kinetics, temperature dependent material behaviour and stress relaxation behaviour of the semi-crystalline polymer [23]. Here, a similar approach is used and the impact of various printing conditions (raster pattern, print bed temperature, layer bonding and layer thickness) with respect to temperature fluctuations and crystallisation on residual stress and warpage of the printed part is studied. The thermo-mechanical properties of the polymer are invoked as a function of temperature for prediction of residual stresses and distortion (warpage) in FDM of semi-crystalline polymers (such as polypropylene) under various printing conditions. COMSOL, a multi-physics software package, is employed as it provides an advanced option for building the required physics for semi-crystalline polymers into the model [34]. Therefore, the part distortion data obtained from this simulation work is influenced by the changes in the thermo-mechanical properties of the polymer (e.g., density), crystallisation and residual stresses, as a result of changes in temperature under various printing conditions. To track the changes in crystallisation degree, residual stresses and warpage during the 3D-printing process with time and temperature, an element of the simulated model is selected and analysed under each printing condition. The warpage values from the developed models are validated with 3D scan of printed parts.

2. Materials and methods

2.1. Process parameters

Polypropylene (PP) provided by 3DFilaprint was selected as the choice of material for this study. PP is a commercially important polymer with crystallisation behaviour that is very sensitive to the applied cooling conditions and is therefore a good material for study. The samples were printed using an Ultimaker 2 with the following printing parameters: nozzle velocity (V) of 30mm/s, nozzle diameter 0.8mm, ambient temperature of 25°C and infill of 100% (since the part would be more prone to shrinkage/warpage with 100%). The crystallisation temperature of the incorporated PP is 160°C. Printed sample dimensions were scanned using an Absolute arm (8525 model) with a RS6 scanner.

The processing parameters for various samples in the simulation are presented in Table 1. In the present study, the FDM processing parameters such as layer thickness (sample c-L_t), bed temperature (sample d-T_b) and raster patterns (sample e-R_p) are varied, and the results are

compared with the reference sample (sample a-R_s). Among the printing parameters listed in Table 1, layer bonding condition is only a FEM assumption and cannot be referred to as a printing condition for sample b-L_b. This assumption was considered to observe the influence of boundary conditions applied between the layers in the model (FEM) over part distortion.

Table 1. Processing parameters and layer bonding condition for polypropylene

Processing conditions	**Extrusion temperature (T_m) (°C)**	**Bed temperature (T_b) (°C)**	**Layer thickness (L_t) (mm)**	**Layer bonding assumption**	**Raster pattern**
Sample a-R_s	210	100	0.5	Perfect	Line
Sample b-L_b	210	100	0.5	Freedom to warp	Line
Sample c-L_t	210	100	0.1	Perfect	Line
Sample d-T_b	210	60	0.5	Perfect	Line
Sample e-R_p	210	100	0.5	Perfect	Zigzag

2.2. Modelling approach

The work presented here is a multi-physics simulation study comprised of solid mechanics, heat transfer and polymer crystallisation kinetics. The physics in the simulation are coupled through the function of temperature (T), allowing intercommunication as the model is cooled and reheated. In order to represent the deposition process in FDM, an in-house built tool path program file was interpolated with the part geometry. This activates the elements in the model with respect to their material deposition according to raster angle and printing pattern progressively. In the heat study, the thermo-mechanical material parameters such as specific heat capacity (C_P), density (ρ) and thermal conductivity (λ) are expressed as a function of temperature (T). This allows the thermo-mechanical properties of the model to change continuously from the time the material is deposited until it cools down to the ambient

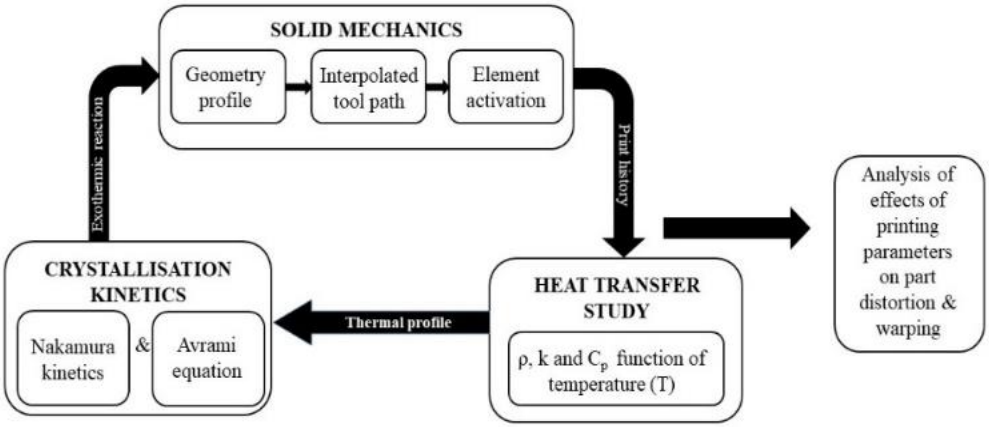

Figure 1. Process simulation plan

temperature. The data from the thermal study is then transferred to crystallisation kinetics which includes the crystallisation phenomenon equations.

Due to the complex nature of the physics involved and duration of the simulation processing time, samples of dimensions of 50 x 50 x 0.4 mm and 50 x 50 x 2 mm were modelled. Figure 1 illustrates the simulation plan in the present study by coupling of crystallisation physics with solid mechanics and heat transfer through the temperature (T). The details of the applied physics and crystallisation kinetics are explained in the next sections. The material characteristics such as the thermo-mechanical properties of the semi-crystalline polymer (C_P, ρ, λ) are expressed as a function of temperature (T) based on the model developed by R. Le Geoff et. al. [35]. For incorporation of crystallisation kinetics into the simulation, the physics developed by Levy A [34] was modified for Polypropylene and used in this study. Also, several other parameters such as the effect of gravity on the deposited filament, contact between the deposited layers, the print bed and ambient temperatures and the viscoelastic nature of the polymer are considered in this present work.

2.3. Physics interfaces

2.3.1. Solid mechanics

In COMSOL, the elements can be activated with respect to heat source, material deposition, temperature, or time. In this study, the elements are activated with respect to material deposition from the nozzle as represented in ***Figure 2***. This is achieved by importing an in-house built tool path file into the model and activating the elements based on the raster pattern. In the simulation, the solid mechanics study invokes the element activation technique to represent the FDM process. The activation initiates when the first element is deposited, and it progresses as the nozzle moves in the x and y axes. After the first layer has been deposited, the print bed moves in the z axis and the deposition continues with a new layer (n_i).

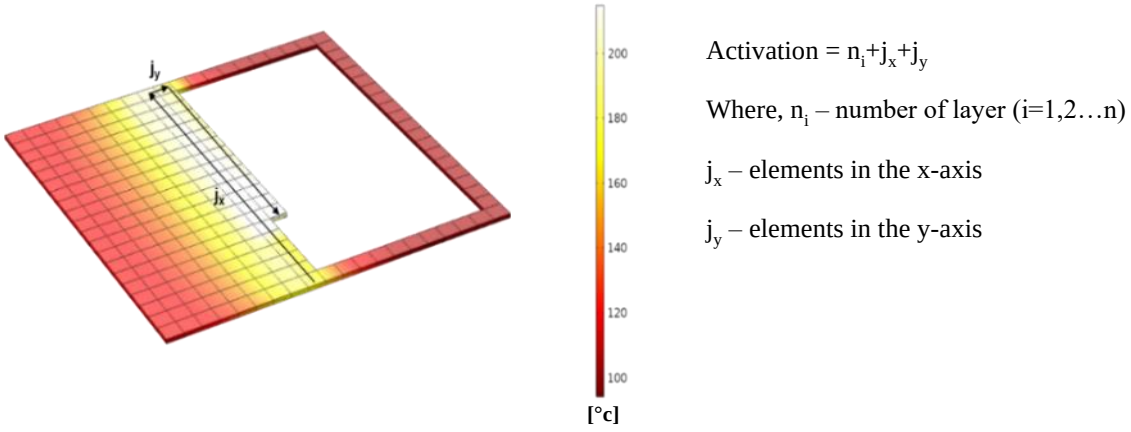

Figure 2. Representation of element activation with respect to the material deposition

The model is meshed according to the size of the deposition of an element from the nozzle. Therefore, during activation an element of 0.5mm size will be activated representing a 0.5mm droplet from the nozzle and a similar approach is taken for the sample with layer thickness of 0.1mm. For the tool path, unidirectional infill (90°/90°) and (45°/45°) was selected and simulated in this study. In order to simplify the simulation, a fixed temperature boundary condition was applied to the bottom layer to resemble the print bed. For boundary conditions, a spring foundation was used as it allows the bottom layer to deform and warp, offering the model the degree of freedom to detach from the build plate. This approach has been successfully undertaken and reported by Courter et al. [29].

To simulate the thermo-viscoelastic nature of the polymer, the Generalised Maxwell (GM) model has been considered. The series of spring-dashpot pairs in GM model represents the polymer chains of the semi-crystalline polymer. The GM model has been widely used among the various constitutive models of linear viscoelastic materials for polymers [36]. The GM model under stress is expressed as:

$$\sigma(t) = \sigma_0 \exp\left(-\frac{t}{\tau_m}\right) \quad (1)$$

Here, σ_0 is the initial stress at t=0 and τ_m is the relaxation time constant. The modulus of the elastic spring (G_0) and the dashpot viscosity (η_0) of the GM model can be written as:

$$\tau_m = \frac{\eta_0}{G_0} \quad (2)$$

The Prony series of relaxation shear modulus function is expressed as follows [36]:

$$G(t) = G_\infty + \sum_{i=1}^{n} G_m exp\left(-\frac{t}{\tau_{mi}}\right) \quad (3)$$

Where, G_∞ is the modulus at infinite time, G_m is the elastic modulus of the spring, τ_{mi} is the relaxation time constant of the spring-dashpot pair in the same branch and n is the total number of maxwell units in the model. The instantaneous shear modulus is defined as:

$$G(t) = G_\infty + \sum_{i=1}^{n} G \quad (4)$$

The viscoelastic property is interpolated with temperature (T) by the consideration of the relaxation time of the material as $\alpha_T(T)\tau_{mi}$, where $\alpha_T(T)$ is a shift function. Williams-Landel-Ferry (WLF) model is commonly used for polymer melts that have a glass transition temperature (T_0). The WLF equation is written as [36]:

$$\log(\alpha_T) = \frac{-C_1(T-T_0)}{C_2+(T-T_0)} \quad (5)$$

Where, C_1 and C_2 are constants that are material dependent.

2.3.2. Heat transfer study

In the past, researchers have continuously emphasised the importance of heat transfer in predicting the thermal history during a FDM process [37]. Primarily, the heat transfer phenomenon in a crystallisation process is exothermic, where the dissipation of heat is continuous. In other words, temperature is the driving factor of the crystallisation process. Therefore, it is imperative to couple temperature (T) with solid mechanics and crystallisation kinetics physics. In this transient heat transfer study, boundary conditions for thermal diffusion such as heat flux, convection between the model and the print bed, heat conduction between the deposited elements and the layers are considered. The general energy balance for the heat transfer considered in the model is presented in equation 1 [35]:

$$\rho C_p \frac{\partial T}{\partial t} - \nabla.(\lambda \nabla T) = Q \qquad (6)$$

Where ρ is the density, $C_p$is the specific heat capacity and λ is the thermal conductivity of the polymer and Q is the heat source.

During the printing process the elements are deposited on the print bed at the melt temperature of 210°C and ambient temperature of 25°C at its respective print bed temperature. The heat from the printed material radiates and is distributed through the nearby elements including the build plate. As a result, the temperature from the newly deposited element affects the previously deposited element leading to a reheating effect, where an element that has already been deposited and on the process of cooling gets reheated. This constant variation in the thermal behaviour of the polymer leads to the development and release of internal stresses inside the polymer [38,39]. Since polymers are inherently poor thermal conductors [4], along with the layer deposition, the influence of the reheating effect from the newly deposited layers reaching the bottom layers would decrease drastically. Therefore, on cooling, the solidified bottom layers of the printed part exhibits high amount of accumulated residual stress leading to part distortion [38,39].

2.3.3 Crystallisation kinetics

This study focuses on the thermo-mechanical properties of the polymer to promote the quantitative prediction of the simulation. The thermo-mechanical properties includes thermal conductivity (λ), specific heat capacity (C_p) and density (ρ), which fundamentally affect the rate of the crystallisation process of a semi-crystalline polymer [40]. Dressler et al. [41] and Wiria et al. [42] have reported that changes in the thermo-mechanical properties can greatly influence the thermal gradient in a polymer. Therefore, C_P, ρ, λ, have been coupled with temperature and invoked into the simulation as expressions. Heat capacity (C_P), density (ρ) and

thermal conductivity (λ) are described using simple mixing rule between the solid and liquid state values weighted by the relative crystallinity.

$$C_p(\alpha, T) = \alpha C_{psc}(T) + (1 - \alpha) C_{pa}(T) \qquad (7)$$

$$\lambda(\alpha, T) = \alpha \lambda_{sc}(T) + \lambda_a(T) \quad (8)$$

$$\rho(P, \alpha, T) = \alpha \rho_{sc}(T) + (1 - \alpha) \rho_a(T) \qquad (9)$$

Here density is inversely proportional to the specific volume of the polymer and has been derived from the PVT diagram [35].

The expressions for polypropylene's amorphous and semi-crystalline regions given in Table 2 are defined by the general equations (7), (8) and (9).

Table 2. Material properties of PP [35]

Thermal property for amorphous (a) and semi-crystalline (sc) states	**Numerical equation**
$C_{pa}(\alpha, T)$	3.1 T + 2124
$\lambda_a(\alpha, T)$	$-$ 6.25 x 10^{-5} T + 0.189
$\rho_a(\alpha, T)$	1 / (1.138 + 6.773 × 10^{-4} T)
$C_{psc}(\alpha, T)$	10.68 T + 1451
$\lambda_{sc}(\alpha, T)$	$-$ 4.96 x 10^{-4} T + 0.31
$\rho_{sc}(\alpha, T)$	1 / (1.077 + 4.225 × 10^{-4} T)

Where, a and sc annotations represent the amorphous region and semi-crystalline regions of the polymer. The melting temperature of the incorporated PP is 210°C with the crystallisation temperature of 160°C. In these equations, the corresponding material property changes with respect to the temperature and the phase change of the polymer.

Avrami proposed an equation which has been widely used to express the crystallisation phenomenon in polymers under isothermal condition [43]:

$$\alpha(t) = 1 - exp\,(-kt^n) \qquad (10)$$

Later considering non-isothermal crystallisation conditions Nakamura proposed a theory deriving from Avrami's equation [43]:

$$\alpha(t) = 1 - exp\left[-\int_0^t K(T)dt\right]^n \qquad (11)$$

Where t is time, n is Avrami index and *K*(T) is the Nakamura crystallisation kinetics function which is derived from Avrami's isothermal kinetics.

$$K(T) = K(T)^{1/n} \qquad (12)$$

Differentiating equation (3) provides the differential form of Nakamura kinetics which is employed to simulate the crystallisation kinetics of a polymer.

$$\frac{\partial \alpha}{\partial t} = n\,K(T)\,g(\alpha) \qquad (13)$$

$$g(\alpha) = (1-\alpha)(-ln(1-\alpha))^{\frac{n-1}{n}} \quad (14)$$

DSC experiments were carried out for both iso-thermal and non-isothermal conditions by Koscher et al. and K(T) was proposed as [43–45]:

$$K(T) = (\frac{4}{3}\pi N_0(T))^{\frac{1}{3}} G_0 * exp\left(-\frac{U^*}{R(T-T_\infty)}\right) exp\,(-\frac{K_g}{T(T_f-T)}) \quad (15)$$

The values of parameters in K(T) from Koscher, are listed as follows [43]:

$$N_0(T) = exp\,(0.156 * (T_f - T) + 15.1) \quad (16)$$

$G_0 = 2.83*10^2$, $K_g = 5.5*10^5(K^2)$, U* = 6284 J/mol.K, R is the gas constant, $T_f = 210^{\circ}C$, $T_\infty = T_g - 30^{\circ}C$, $\Delta H = 90*10^3 J/kg$ and n = 3.

The Nakamura crystallisation kinetics model was used in this study as it is a widely used to predict the dynamics of crystallisation in a polymer [35,40,46–48]. Due to the invoked crystallisation physics, the required material properties of a semi-crystalline polymer appear in the material properties section of the model. This allows the user to input the semi-crystalline property data of the respective polymer into the model. The built-in physics provides several options such as calculating the degree of crystallisation against time and temperature [45]. When modelling polymer crystallisation kinetics, the degree of transformation α is considered between 0 and 1, where 0 and 1 represents limits for fully amorphous state and fully crystallised polymer. In this study, the crystallisation process is taken into consideration as a factor of both time and temperature to predict the rate of crystallisation in the polymer with respect to each printing condition.

3. Results and discussion

In this study, a specific element is selected from layer 1 to observe and investigate the reheating leads to re-crystallisation, and cold crystallisation effects inside the part model. In the FDM process, the thermal inertia received from the immediate adjacent deposited layers can initiate re-crystallisation in the bottom layers based on the crystallisation temperature of the printed semi-crystalline polymer. During recrystallisation, the solidified polymer crystals are melted and undergo crystallisation process again. However, as the layer deposition progresses, the heat received by the subjacent layers from the newly deposited layers is greatly reduced. Thus, after the deposition of few layers, even though the bottom layer is reheated slightly by the thermal gradient from the newly deposited layers, since the heat received is below the crystallisation temperature of the polymer, it results in cold crystallisation. Reheating of the cooled polymer to above its glassy state (but below its crystallisation temperature) can promote further crystallisation of the polymer molecules. This is regarded as cold crystallisation [49]. The present work mainly focuses on analysing the data from this specific

element in layer 1, in order to study the influence of the processing conditions and crystallisation on the changes in residual stress and warpage of the model. This selected element on layer 1 is referred to as element n (Figure 3(a)) throughout the study.

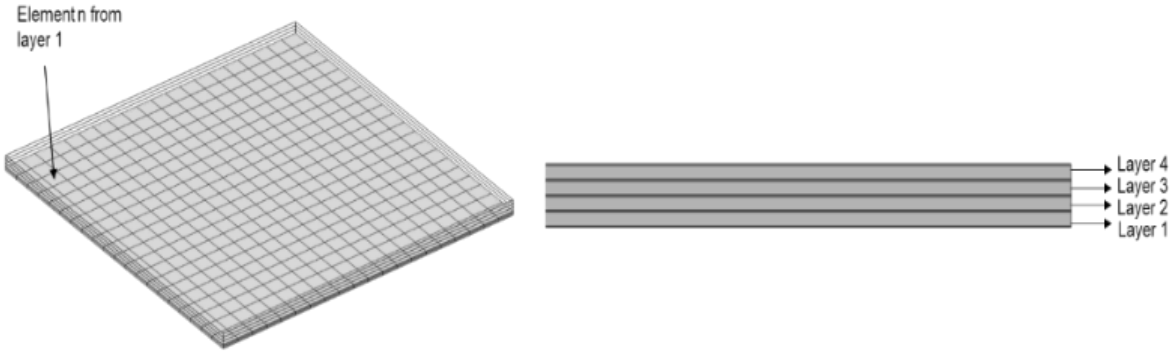

(a) (b)

Figure 3. (a) Iso-metric view and location of element n in the printed part (b) Side view of the printed part representing the layer sequence.

3.1. Temperature evolution during printing

The melted polymer was deposited at 210°C and allowed to cool down until it reaches the bed temperature.

Figure 4 shows the changes in temperature of element n with time over the printing

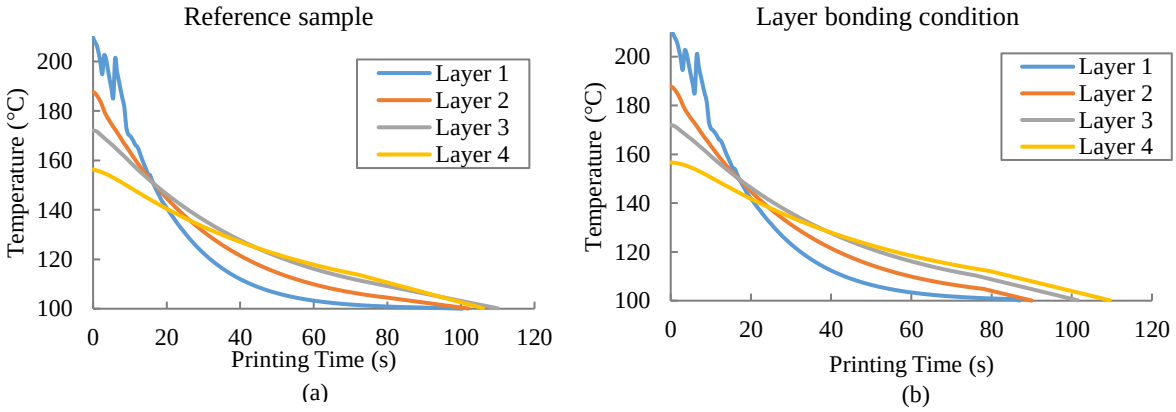

duration. For the printing conditions demonstrated in

Figure 4 (a), (b), (c) and (e) the print bed temperature was fixed at 100°C and for

Figure 4 (d) the print bed temperature was set to 60°C. In order to compare and study the reheating effect of other layers on layer 1, in

Figure 4 the printing time of all the layers are overlapped in the x-axis.

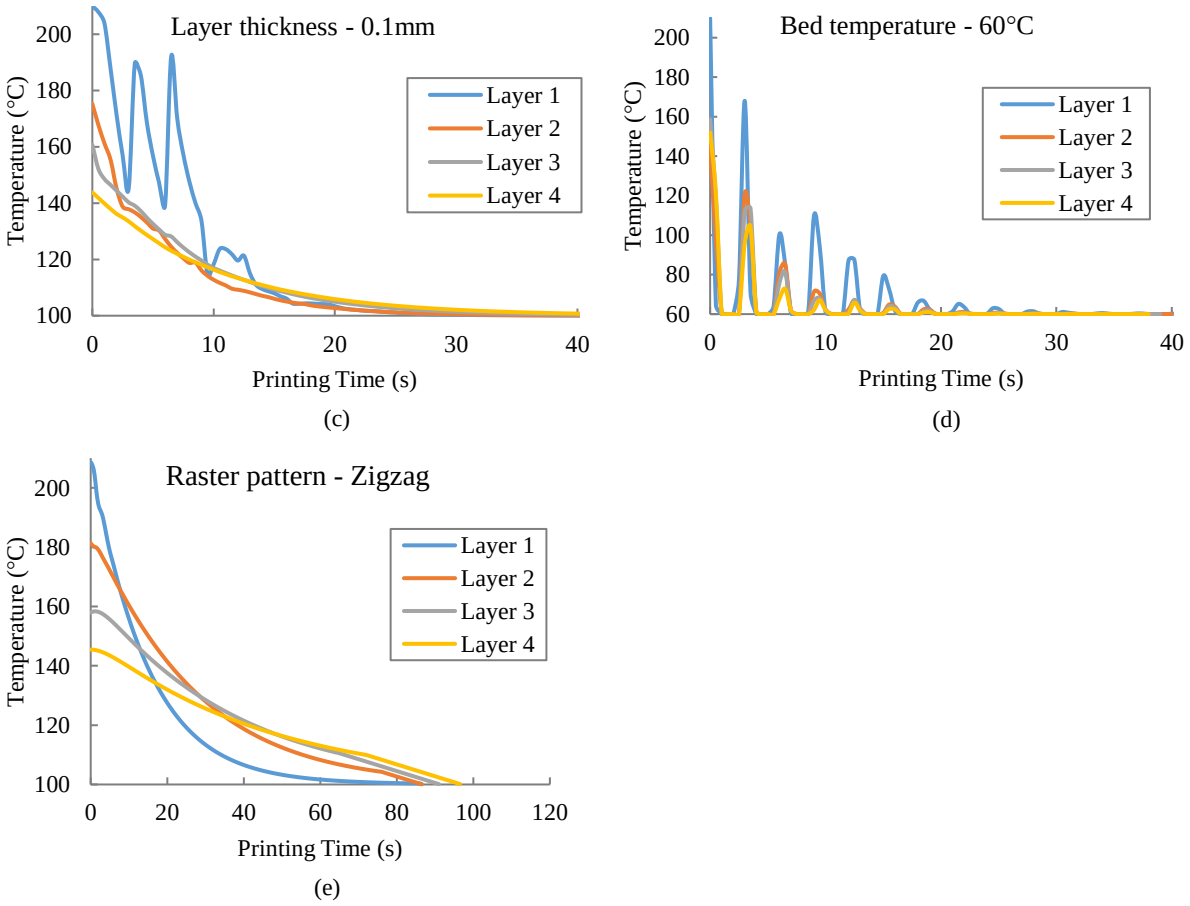

Figure 4. Effect of thermal history from element n with respect to printing time of each layer at various printing conditions. (a) Sample a-R_s, (b) Sample b-L_b, (c) Sample c-L_t, (d) Sample d-T_b and (e) Sample e-R_p.

From

Figure 4, it can be observed from all the samples, that the deposition of element n initiates at 210°C (the melting temperature of the polymer) and cools down as the deposition progresses. During the initial stages of this cooling process, small continuous peaks are observed in layer 1. These peaks are formed as element n undergoes reheating due to the newly deposited neighbouring roads. This behaviour can be seen more clearly in all the samples except sample e-R_p, since sample e-R_p undergoes a different thermal evolution due to the use of a zigzag raster pattern. In sample c-L_t, since the layer thickness of the sample is very small, the thermal inertia from the neighbouring roads significantly affects the cooling rate of element n. Whereas in sample d-T_b, these peaks are evidently visible throughout the printing process and distinguished separately from each other. This is because the newly deposited neighbouring roads in sample d-T_b constantly reheat the roads that have already been deposited and cooled at a rapid rate from 210°C to 60°C (the bed temperature). This reheating effect by the neighbouring roads was also observed in the simulation work reported by Zhang et al. [16] and Spoerk et al. [50]. The bottom layer (layer 1) was also affected by the heat transferred from newly deposited layers. However, layer reheating from subsequent layers does not have a significant influence on element n when compared to the reheating effect from the adjacent road. This was expected, as the heat transfer between the layers reduces with the increase in distance from element n. Since semi-crystalline polymers are poor thermal conductors, the temperature distribution from the top layer to the bottom layer is relatively low [51].

As depicted in

Figure 4, during the overall cooling process of element n in sample a-R_s, sample b-T_a, sample c-L_t and sample e-R_p, the temperature gradient drops more gradually compared to sample d-T_b. Furthermore, among all the samples, sample c-L_t and d-T_b have the least cooling time. Due to the smaller layer thickness condition in sample c-L_t, the printing and the cooling process are faster in this case. For sample d-T_b, since the deposited melt is forced to cool rapidly due to the lower bed temperature printing condition (T_b=60°C), the temperature of the deposited roads (including element n) falls steeply from 210°C to 60°C. Additionally, due to the lower bed temperature it can be observed in sample d-T_b that element n is reheated continuously by both neighbouring roads and newly deposited layers and forced cool. This constant reheating and rapid cooling process affect the cooling period of the bottom layer (layer 1) leading to a build-up of internal residual stresses [2].

3.2. Effects of crystallisation on part distortion

To examine the effect of crystallisation on residual stress and part distortion, the relative crystallinity, warpage, and residual stress of element n are reported in Figure 5 when the temperature reaches 120°C (after completion of the printing process for all the four layers as the sample cools down), with respect to the different printing conditions. The data presented here was selected at 120°C, in order to showcase the relationship between crystallinity, residual stress and warpage for the samples above the bed temperature (100°C) and below the crystallisation temperature of PP (160°C).

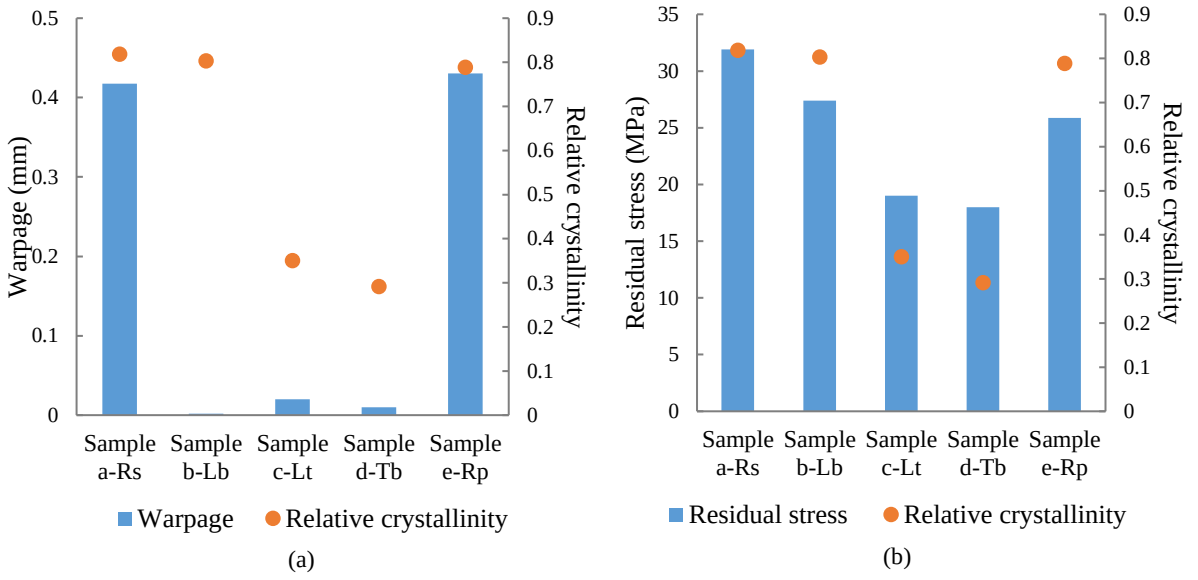

Figure 5. (a) Warpage and relative crystallinity for element n at 120℃ plotted for samples with respect to different printing conditions (b) Residual stress and relative crystallinity for element n at 120℃ plotted for samples with respect to different printing conditions.

In Figure 5, it can be noted that, sample a-R_s and sample e-R_p have the highest relative crystallinity, warpage, and in-built residual stress amongst the samples. The only difference between these two samples is the printing pattern (raster angle). In both cases, the samples cool down slowly by maintaining the bed temperature closer to the crystallisation temperature of the polymer thereby enabling the polymer chains to gradually crystallise from the melt state

and achieving a high degree of crystallinity [4]. Increased levels of crystallinity result in higher shrinkage and therefore an increase in warpage and residual stresses in the part. Even though the relative crystallinity and the built-in residual stress of sample b-L_b is in the same range as sample a-R_s and sample e-R_p, it is found to have the least warpage. This is ascribed to the unconstrained bonding between the layers in this case and freedom for each layer to deform and shear without restriction from other layers, resulting in a reduced overall warpage, despite the high crystallinity in sample b-L_b.

The small layer thickness in sample c-L_t (by an order of one fifth), leads to higher dissipation of heat (i.e., rapid cooling) and consequently a relatively low degree of crystallinity and in-built residual stress, and therefore lower warpage compared with sample a-R_s and sample e-R_p.

In Figure 5, sample d-T_b exhibits the lowest degree of crystallinity with low in-built residual stress and consequently, a very low degree of warpage. As explained in section 3.1, sample d-T_b cools at a much faster rate in comparison to the other samples due to the low print bed temperature. Therefore, due to the higher cooling rate of element n, the polymer crystal growth is highly limited by restricting the energy of polymer chains for alignment and orientation; hence, decreasing the crystallinity, and consequently resulting in low amounts of residual stress and warpage [4,50].

3.3. Residual stress vs printing time

Figure 6 illustrates the development and distribution of residual stresses in element n due to the subsequent deposition of layers (1, 2, 3 and 4) against overall printing time for the various printing conditions. Sample a-R_s, is used as a reference for comparison.

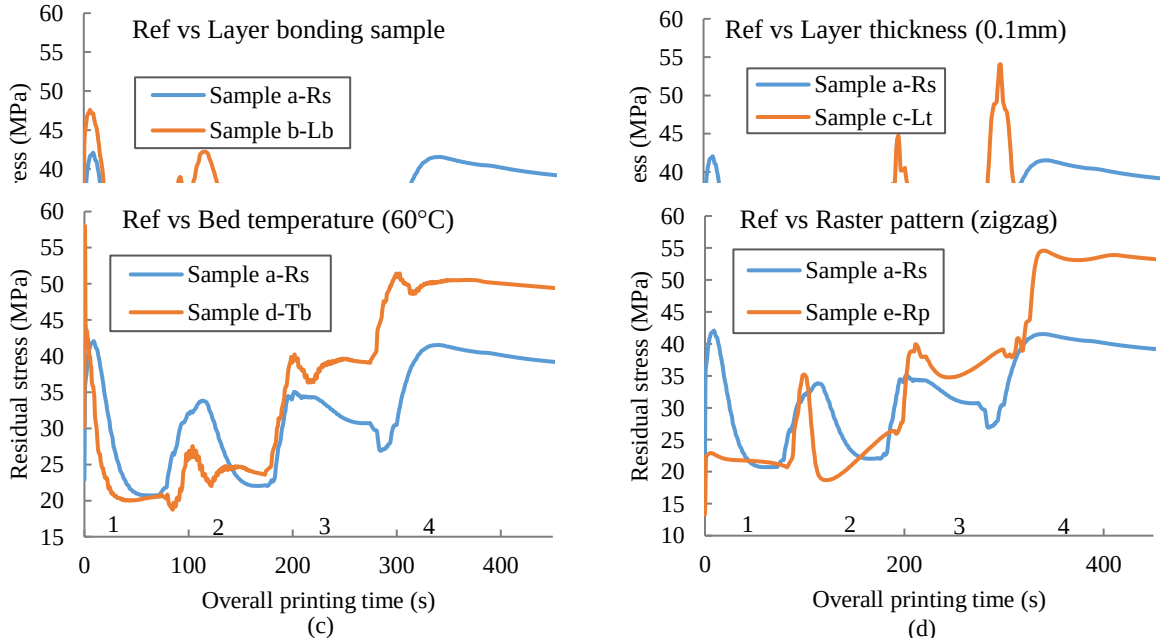

Figure 6. Comparison of residual stress distribution from element n of sample a-R_s with each individual sample plotted against overall printing time. (1) layer 1 (2) layer 2 (3) layer 3 (4) layer 4 are indicated inside the graph for layer reference.

The four main peaks in all the samples in Figure 6, occur due to the large temperature gradients in element n as the molten layers are subsequently deposited. Hence, element n is repeatedly reheated and cooled resulting in the release and build-up of residual stress, respectively. In other words, the residual stress built inside element n is released (i.e., reduced) due to the reheating effect of the newly deposited layer over the subjacent layers in a sample. Once the cooling phase begins, the residual stress starts to build-up again. As illustrated in Figure 6, further growth of residual stresses stops and becomes constant after the printing process is completed and the part is allowed to cool down [38]. The appearance of large prominent peaks in the residual stress in sample c-L_t can be ascribed to the larger heat dissipation and heat transfer within this sample due to its lower layer thickness. The improved heat transfer in this sample can promote cold crystallisation (where the polymer undergoes small amount of crystallisation while heating) and elevate residual stresses. In the other samples, the heat transfer from the top layers to element n in the first layer is considerably lower than in sample c-L_t, due to the higher layer thickness and poor thermal conductivity of the polymer [49,51]. In sample d-T_b the reheating effect and reduction of residual stress in each step is less pronounced due to the rapid cooling effect.

On observation, sample b-L_b and sample c-L_t are found to have the least ultimate residual stress. In sample b-L_b, during the cooling phase, as every layer has the freedom to disconnect from its subjacent layers, the layers can undergo shear and separate from each other. Due to this behaviour, the residual stresses built-in the layers are released resulting in negligible overall warpage of 0.002 mm. Whereas in sample c-L_t, the smaller overall residual stress can be attributed to the larger and more uniform heat transfer within the sample due to the smaller layer thickness, which is in good agreement with the conclusions drawn by Zhang Y [2] and Zhang J [16] stating that stress accumulation increases with an increase in layer thickness of the part.

In contrast to sample b-L_b and c-L_t, the residual stress trend appears to increase continuously with each layer deposition in sample d-T_b and sample e-R_p. The rapid cooling condition in sample d-T_b freezes the residual stress inside the layers as they are printed leading to a steady increase in the induced stresses. In Figure 5, even though sample d-T_b recorded the lowest residual stress and warpage at 120°C, once fully cooled and stabilised, it exhibits the second highest built-in stress among all the samples (Figure 6). The rapid cooling condition

and abrupt change in temperature with cooling time gives rise to continuous accumulation of thermal stress inside the layers [52], thereby leading to significant increase in the residual stress in sample d-T_b. While in sample e-R_p, the reheating of element n by the newly deposited layers is limited to a shorter period of time due to the zigzag raster pattern which leads to a 36% higher residual stress at the end of printing process in comparison to what occurs with the line raster pattern. In a study by Pandzic et al. on FDM, it was reported that the line pattern resulted in 3D printed samples with higher yield strength in relation to the zigzag pattern [53].

3.4. Warpage vs printing time

Warpage is caused due to the anisotropic contraction changes induced by built-in residual stresses [12]. The amount of warpage (part distortion) in the modelled samples are presented in

Figure ***7*** and the influential factors/printing conditions are investigated. Here, warpage

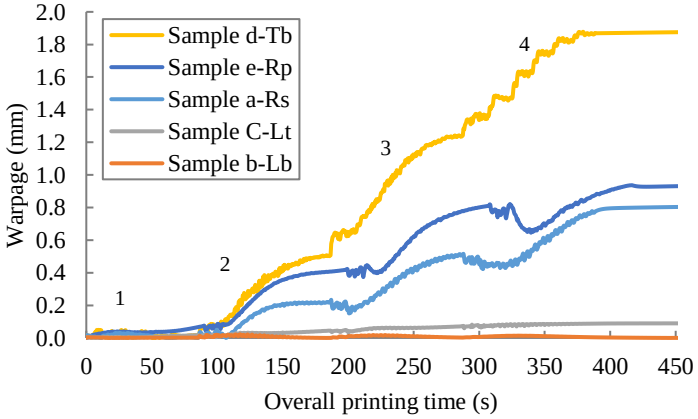

from the samples is plotted against the overall printing time to illustrate the continuous change in part distortion throughout the printing process.

Figure 7. Warpage from element n with respect to consequent layer deposition plotted against over all printing time. (1) layer 1 (2) layer 2 (3) layer 3 (4) layer 4 are indicated inside the graph for layer reference.

As seen in

Figure ***7***, there is a stepwise increase in the amount of warpage in element n with printing time in accordance with the progression of layer deposition and the resultant heat transfer. As discussed previously in section 3.2., the reheating effect of element n by the newly deposited layers results in a slight reduction of warpage. This effect is seen more clearly in sample a-R_s and sample e-R_p.

Sample b-L_b has the lowest warpage followed by sample c-L_t with the second lowest warpage value. Zhang et al. [2] and Sahu et al. [54] in their study concluded that reducing layer thickness can increase the dimensional accuracy of a printed part in the z-direction which correlates with the warpage results of this study. Also, from

Figure 7, it can be concluded that the stress accumulation in the model increases with an increase in layer thickness [2,16]. So, it is imperative to consider layer thickness as a significant factor in warping. The effect of layer-layer bonding on part distortion has not been assessed experimentally.

As described in section 3.3, the continuous increase in residual stress in sample d-T_b as it cools down and stabilises results in high amount of warpage (

Figure 7). Due to the rapid cooling in this sample, the mobility of the polymer chains reduces drastically, resulting in higher accumulation of residual stresses inside the layers and inducing significant amount of warpage [55]. Sample e-R_p shows a 16% increase in warpage in comparison to sample a-R_s due to the increased built-in residual stress (as discussed in section 3.2).

While crystallisation, residual stress and warpage data of all the samples in Figure 5 were plotted at 120°C for element n after the final layer of the samples were printed, here the final residual stress and overall warpage of the samples once they reach steady state and stabilised (after completion of the printing process) are plotted in Figure 8. It is evident that there is a consistency between the amount of residual stress and warpage with an increase in residual stress resulting in an increase in warpage.

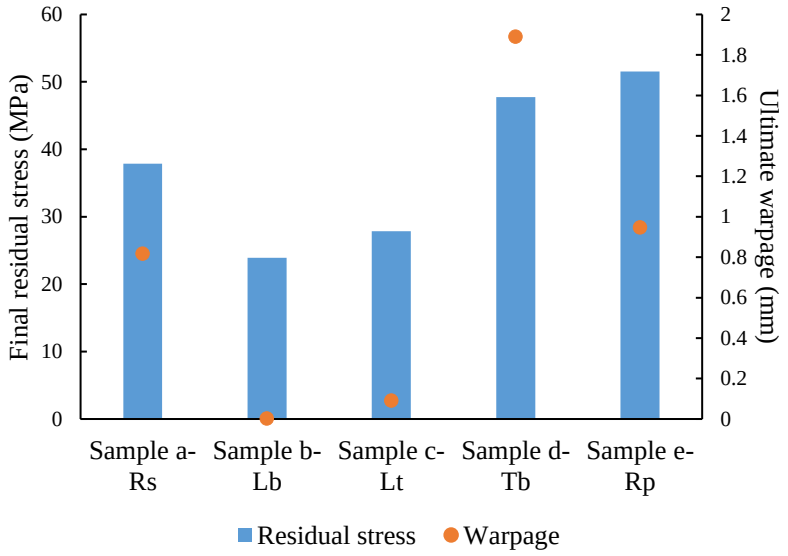

Figure 8. Final residual stress of samples printed under various printed conditions are plotted against the Ultimate warpage to illustrate the effect of residual stress on part warpage.

In Figure 8, it can be noted that while sample c-L_t exhibits 26% decrease in residual stress and 89% drop in warpage when compared to sample a-R_s, sample d-T_b demonstrates an increase of 26% residual stress followed with a significant increase of 131% warpage. On comparison with sample a-R_s, sample e-R_p shows 36% increase in residual stress resulting in 16% increase in warpage. It should be noted that each sample (printed/simulated) is only compared with sample a-R_s (reference sample) to assess the effect of each printing condition. From Figure 8, it can be clearly noted here that the warpage is greatly affected by the residual stresses of the samples and there is a direct relationship between them.

3.5. Experimental validation

The warpage results from the samples c-L_t and d-T_b were validated by comparing with the respective 3D scanned data of printed samples. Samples d-T_b and c-L_t with the highest and lowest warping were selected in order to assess the reliability of the model's prediction. Since the warpage of element n was measured, the printed sample was scanned and overlapped on the 3D model. Following this, a cartesian co-ordinate was created from the CAD model at (0,0,0) while another axis was created at element n. The warpage values are measured here by comparing the deviation values obtained from the nominal axis (0,0,0) and the axis at element n.

Figure 10 shows the warpage comparison between the simulated sample d-T_b and 3D scan result. In both Figure 9 (a) and (b), the sample detaches from the print bed with warping on the edges implying the significance of bed temperature and geometry (in this case) in influencing part distortion [19].

Figure 10. Representation of warpage results between simulated and 3D printed sample d-Tb.

Table 3. Experimental validation of the simulated sample warpage of element n

Samples	Predicted warpage (FEA) (mm)	Measured warpage (Experimental) (mm)	Deviation (%)
Sample c-L_t	0.09	0.093	-3.22%
Sample d-T_b	1.89	1.95	-3.1%

In Table 3, the warpage data from element n in samples c-L_t and d-T_b are compared with their 3D printed part warpage results. It is evident that the predicted warpage value from the developed simulation is in a very good agreement with the experimentally measured value.

4. Conclusion

In this study, the temperature evolution of the printed sample and the crystallisation of the polymer has been simulated using FEA and crystallisation physics. The effect of printing parameters such as bed temperature, layer thickness, layer bonding and raster pattern on warping and in-built residual stress has been considered. Based on the simulation results, a line raster pattern produces a drop of 16% in warpage and 36% in residual stress in comparison with a zigzag raster pattern. Decreasing the layer thickness of the model from 0.5mm to 0.1mm results in a decrease in warpage of 89%.

From the simulation, it has been observed that the residual stress in the 3D printed part is significantly influenced by the semi-crystalline physics and temperature dependency of the thermo-mechanical properties of the polymer. This approach has provided insight into the relationship between printing conditions, crystallisation, residual stresses, and warpage in FDM printed parts, leading to quantitative predictions of part distortion. It clearly indicates that using a smaller layer size has a significant, positive effect on reducing warpage.

The warpage predicted from the simulated model was validated with the experimentally obtained 3D scanned data from a printed part. The model displayed a deviation of less than 4%, thus showing the validity of the model in predicting part warpage. The results of this study can be used to predict and understand the effect of printing parameters and polymer properties on residual stresses and warpage during FDM of a semi-crystalline polymer to minimise shrinkage/warpage in a 3D-printed part.

5. Future work

As an extension to this study, other printing parameters such as nozzle speed, sample height, ambient temperature and various raster patterns will be simulated to study their effects on warpage and residual stresses. Additionally, the effect of adding filler in polymer matrix and concentration will be taken into account to predict part distortion in composite material during FDM.

Acknowledgements

The North West Centre for Advanced Manufacturing (NW CAM) project is supported by the European Union's INTERREG VA Programme, managed by the Special EU Programmes Body (SEUPB). The views and opinions in this document do not necessarily reflect those of the European Commission or the Special EU Programmes Body (SEUPB). If you would like further information about NW CAM, please contact the lead partner, Catalyst, for details. I would extend my thanks to Monali Dahale, Sean Duffy, William Moses and COMSOL for their support. The authors would also like to thank GH Inspection for providing the 3D scan facility.

References

[1] H. Bikas, P. Stavropoulos, G. Chryssolouris, Additive manufacturing methods and modeling approaches: A critical review, Int. J. Adv. Manuf. Technol. 83 (2016) 389–405. https://doi.org/10.1007/s00170-015-7576-2.

[2] Y. Zhang, K. Chou, A parametric study of part distortions in fused deposition modelling using three-dimensional finite element analysis, Proc. Inst. Mech. Eng. Part B J. Eng. Manuf. 222 (2008) 959–967. https://doi.org/10.1243/09544054JEM990.

[3] N. Yu, X. Sun, Z. Wang, D. Zhang, J. Li, Effects of auxiliary heat on warpage and mechanical properties in carbon fiber/ABS composite manufactured by fused deposition modeling, Mater. Des. 195 (2020) 108978. https://doi.org/10.1016/j.matdes.2020.108978.

[4] J. John R. Wagner, Jr., Eldridge M. Mount, III and Harold F. Giles, Extrusion The Definitive Processing Guide and Handbook, 2013. https://doi.org/https://doi.org/10.1016/C2010-0-67040-4.

[5] P.K. Penumakala, J. Santo, A. Thomas, A critical review on the fused deposition modeling of thermoplastic polymer composites, Compos. Part B Eng. 201 (2020) 108336. https://doi.org/10.1016/j.compositesb.2020.108336.

[6] A. Golbang, E. Harkin-Jones, M. Wegrzyn, G. Campbell, E. Archer, A. McIlhagger, Production and characterization of PEEK/IF-WS2 nanocomposites for additive manufacturing: Simultaneous improvement in processing characteristics and material properties, Addit. Manuf. 31 (2020) 100920. https://doi.org/10.1016/j.addma.2019.100920.

[7] C.Y. Li, The rise of semicrystalline polymers and why are they still interesting, Polymer (Guildf). 211 (2020) 123150. https://doi.org/10.1016/j.polymer.2020.123150.

[8] Y. Zhang, Y. Chou, Three-dimensional finite element analysis simulations of the fused

deposition modelling process, Proc. Inst. Mech. Eng. Part B J. Eng. Manuf. 220 (2006) 1663–1671. https://doi.org/10.1243/09544054JEM572.

[9] A. Siegmann, A. Buchman, S. Kenig, Residual stresses in polymers I: The effect of thermal history, Polym. Eng. Sci. 21 (1981) 40–47. https://doi.org/10.1002/pen.760220107.

[10] W.F. Zoetelief, L.F.A. Douven, A.J. Ingen Housz, Residual thermal stresses in injection molded products, Polym. Eng. Sci. 36 (1996) 1886–1896. https://doi.org/10.1002/pen.10585.

[11] F. Bähr, E. Westkämper, Correlations between Influencing Parameters and Quality Properties of Components Produced by Fused Deposition Modeling, Procedia CIRP. 72 (2018) 1214–1219. https://doi.org/10.1016/j.procir.2018.03.048.

[12] T. Koslowski, C. Bonten, Shrinkage, warpage and residual stresses of injection molded parts, AIP Conf. Proc. 2055 (2019). https://doi.org/10.1063/1.5084847.

[13] L.B. Ji, T.R. Zhou, Finite Element Simulation of Temperature Field in Fused Deposition Modeling, Adv. Mater. Res. 97–101 (2010) 2585–2588. https://doi.org/10.4028/www.scientific.net/AMR.97-101.2585.

[14] K. Nakamura, T. Watanabe, K. Katayama, T. Amano, Some aspects of nonisothermal crystallization of polymers. I. Relationship between crystallization temperature, crystallinity, and cooling conditions, J. Appl. Polym. Sci. 16 (1972) 1077–1091. https://doi.org/10.1002/app.1972.070160503.

[15] A. Jungmeier, G.W. Ehrenstein, D. Drummer, New aspects of process induced properties of microinjection moulded parts, Plast. Rubber Compos. 39 (2010) 308–314. https://doi.org/10.1179/174328910X12691245470392.

[16] J. Zhang, X.Z. Wang, W.W. Yu, Y.H. Deng, Numerical investigation of the influence of process conditions on the temperature variation in fused deposition modeling, Mater. Des. 130 (2017) 59–68. https://doi.org/10.1016/j.matdes.2017.05.040.

[17] S. Hertle, M. Drexler, D. Drummer, Additive Manufacturing of Poly(propylene) by Means of Melt Extrusion, Macromol. Mater. Eng. 301 (2016) 1482–1493. https://doi.org/10.1002/mame.201600259.

[18] O.S. Carneiro, A.F. Silva, R. Gomes, Fused deposition modeling with polypropylene, Mater. Des. 83 (2015) 768–776. https://doi.org/10.1016/j.matdes.2015.06.053.

[19] J.P. Hämäläinen, Semi-Crystalline Polyolefins in Fused Deposition Modeling, 2017. https://pdfs.semanticscholar.org/297d/740e376e45a23216abe5091a6337cd0e8023.pdf.

[20] A. Armillotta, M. Bellotti, M. Cavallaro, Warpage of FDM parts: Experimental tests

and analytic model, Robot. Comput. Integr. Manuf. 50 (2018) 140–152. https://doi.org/10.1016/j.rcim.2017.09.007.

[21] L. Wang, J.E. Sanders, D.J. Gardner, Y. Han, Effect of fused deposition modeling process parameters on the mechanical properties of a filled polypropylene, Prog. Addit. Manuf. 3 (2018) 205–214. https://doi.org/10.1007/s40964-018-0053-3.

[22] M. Spoerk, F. Arbeiter, I. Raguž, G. Weingrill, T. Fischinger, G. Traxler, S. Schuschnigg, L. Cardon, C. Holzer, Polypropylene Filled With Glass Spheres in Extrusion-Based Additive Manufacturing: Effect of Filler Size and Printing Chamber Temperature, Macromol. Mater. Eng. 303 (2018). https://doi.org/10.1002/mame.201800179.

[23] B. Brenken, E. Barocio, A. Favaloro, V. Kunc, R.B. Pipes, Development and validation of extrusion deposition additive manufacturing process simulations, Addit. Manuf. 25 (2019) 218–226. https://doi.org/10.1016/j.addma.2018.10.041.

[24] T. Glomsaker, Å. Larsen, E. Andreassen, E. Ommundsen, Experimental and numerical investigation of warpage of semicrystalline polymers in rotational molding, Polym. Eng. Sci. 45 (2005) 945–952. https://doi.org/10.1002/pen.20348.

[25] H. Xu, C.T. Bellehumeur, Thermal residual stress development for semi-crystalline polymers in rotational molding, Polym. Eng. Sci. 48 (2008) 283–291. https://doi.org/10.1002/pen.20887.

[26] E.Q. Clutton, J.G. Williams, On the measurement of residual stress in plastic pipes, Polym. Eng. Sci. 35 (1995) 1381–1386. https://doi.org/10.1002/pen.760351709.

[27] A.J. Favaloro, B. Brenken, E. Barocio, R.B. Pipes, Simulation of Polymeric Composites Additive Manufacturing using Abaqus, Sci. Age Exp. (2017) 103–114. https://www.3ds.com/fileadmin/PRODUCTS/SIMULIA/PDF/scc-papers/2017/simulation-polymeric-composites-am-purdue-favalaro.pdf.

[28] R. Spina, M. Spekowius, R. Dahlmann, C. Hopmann, Analysis of polymer crystallization and residual stresses in injection molded parts, Int. J. Precis. Eng. Manuf. 15 (2014) 89–96. https://doi.org/10.1007/s12541-013-0309-2.

[29] B. Courter, V. Savane, J. Bi, S. Dev, C.J. Hansen, Finite Element Simulation of the Fused Deposition Modelling Process Modelling Process, (2017).

[30] H.S. Ramanath, C.K. Chua, K.F. Leong, K.D. Shah, Melt flow behaviour of poly-ε-caprolactone in fused deposition modelling, J. Mater. Sci. Mater. Med. 19 (2008) 2541–2550. https://doi.org/10.1007/s10856-007-3203-6.

[31] A. D'Amico, A.M. Peterson, An adaptable FEA simulation of material extrusion

additive manufacturing heat transfer in 3D, Addit. Manuf. 21 (2018) 422–430. https://doi.org/10.1016/j.addma.2018.02.021.

[32] B.B. Shahriar, C. Arthur, C. France, N. Valérie, Influence of parameters controlling the extrusion step in fused filament fabrication (FFF) process applied to polymers using numerical simulation, AIP Conf. Proc. 1960 (2018). https://doi.org/10.1063/1.5034995.

[33] T.E. Gartner, A. Jayaraman, Modeling and Simulations of Polymers: A Roadmap, Macromolecules. 52 (2019) 755–786. https://doi.org/10.1021/acs.macromol.8b01836.

[34] A. Levy, Robust Numerical Resolution of Nakamura Crystallization Kinetics, Int. J. Theor. Appl. Math. 3 (2017) 143. https://doi.org/10.11648/j.ijtam.20170304.13.

[35] R. Le Goff, G. Poutot, D. Delaunay, R. Fulchiron, E. Koscher, Study and modeling of heat transfer during the solidification of semi-crystalline polymers, Int. J. Heat Mass Transf. 48 (2005) 5417–5430. https://doi.org/10.1016/j.ijheatmasstransfer.2005.06.015.

[36] Q. Xu, B. Engquist, M. Solaimanian, K. Yan, A new nonlinear viscoelastic model and mathematical solution of solids for improving prediction accuracy, Sci. Rep. 10 (2020) 1–10. https://doi.org/10.1038/s41598-020-58240-y.

[37] D. Popescu, A. Zapciu, C. Amza, F. Baciu, R. Marinescu, FDM process parameters influence over the mechanical properties of polymer specimens: A review, Polym. Test. 69 (2018) 157–166. https://doi.org/10.1016/j.polymertesting.2018.05.020.

[38] A. El Moumen, M. Tarfaoui, K. Lafdi, Modelling of the temperature and residual stress fields during 3D printing of polymer composites, Int. J. Adv. Manuf. Technol. (2019) 1661–1676. https://doi.org/10.1007/s00170-019-03965-y.

[39] H. Xia, J. Lu, S. Dabiri, G. Tryggvason, Fully resolved numerical simulations of fused deposition modeling. Part I: fluid flow, Rapid Prototyp. J. 24 (2018) 463–476. https://doi.org/10.1108/RPJ-12-2016-0217.

[40] A. Levy, S. Le Corre, V. Sobotka, Heat transfer and crystallization kinetics in thermoplastic composite processing. A coupled modelling framework, AIP Conf. Proc. 1769 (2016). https://doi.org/10.1063/1.4963594.

[41] M. Dressler, M. Röllig, M. Schmidt, A. Maturilli, J. Helbert, Temperature distribution in powder beds during 3D printing, Rapid Prototyp. J. 16 (2010) 328–336. https://doi.org/10.1108/13552541011065722.

[42] F. Edith Wiria, K. Fai Leong, C. Kai Chua, Modeling of powder particle heat transfer process in selective laser sintering for fabricating tissue engineering scaffolds, Rapid

Prototyp. J. 16 (2010) 400–410. https://doi.org/10.1108/13552541011083317.

[43] E. Koscher, R. Fulchiron, Influence of shear on polypropylene crystallization: Morphology development and kinetics, Polymer (Guildf). 43 (2002) 6931–6942. https://doi.org/10.1016/S0032-3861(02)00628-6.

[44] N. Brahmia, P. Bourgin, M. Boutaous, D. Garcia, Numerical simulation with "Comsol Multiphysics" of crystallization kinetics of semi-crystalline polymer during cooling: Application to injection moulding, Comsol Users Conf. (2006) 1–7. http://www.comsol.eu/papers/1575/download/Brahmia.pdf.

[45] A. Levy, A Novel Physics Node for Nakamura Crystallization Kinetics, Int. J. Numer. Methods Eng. (2016). https://doi.org/10.1002/nme.

[46] N. Boyard, Heat Transfer in Polymer Composite Materials: Forming Processes, Heat Transf. Polym. Compos. Mater. Form. Process. (2016) 1–434. https://doi.org/10.1002/9781119116288.

[47] B. Pignon, X. Tardif, N. Lefèvre, V. Sobotka, N. Boyard, D. Delaunay, A new PvT device for high performance thermoplastics: Heat transfer analysis and crystallization kinetics identification, Polym. Test. 45 (2015) 152–160. https://doi.org/10.1016/j.polymertesting.2015.05.013.

[48] F. Amado, K. Wegener, M. Schmid, G. Levy, Characterization and modeling of non-isothermal crystallization of Polyamide 12 and co-Polypropylene during the SLS process, 5th Int. Polym. Mould. Innov. Conf. (2012) 207–216.

[49] Y. Furushima, C. Schick, A. Toda, Crystallization, recrystallization, and melting of polymer crystals on heating and cooling examined with fast scanning calorimetry, Polym. Cryst. 1 (2018) 1–10. https://doi.org/10.1002/pcr2.10005.

[50] M. Spoerk, C. Holzer, J. Gonzalez-Gutierrez, Material extrusion-based additive manufacturing of polypropylene: A review on how to improve dimensional inaccuracy and warpage, J. Appl. Polym. Sci. (2019).

[51] A.B. Robbins, A.J. Minnich, Crystalline polymers with exceptionally low thermal conductivity studied using molecular dynamics, Appl. Phys. Lett. 107 (2015). https://doi.org/10.1063/1.4936195.

[52] R.T.L. Ferreira, R. Quelho de Macedo, Residual thermal stress in fused deposition modelling, (2018). https://doi.org/10.26678/abcm.cobem2017.cob17-0124.

[53] A. Pandzic, D. Hodzic, A. Milovanovic, Effect of infill type and density on tensile properties of pla material for fdm process, Ann. DAAAM Proc. Int. DAAAM Symp. 30 (2019) 545–554. https://doi.org/10.2507/30th.daaam.proceedings.074.

[54] R.K. Sahu, S.S. Mahapatra, A.K. Sood, A Study on Dimensional Accuracy of Fused Deposition Modeling (FDM) Processed Parts using Fuzzy Logic, J. Manuf. Sci. Prod. 13 (2014) 183–197. https://doi.org/10.1515/jmsp-2013-0010.

[55] S.F. Costa, F.M. Duarte, J.A. Covas, Estimation of filament temperature and adhesion development in fused deposition techniques, J. Mater. Process. Technol. 245 (2017) 167–179. https://doi.org/10.1016/j.jmatprotec.2017.02.026.